Editors' Suggestion

Visualizing the Kondo lattice crossover in $YbRh_2Si_2$ with Compton scattering

M. Güttler[1,*] K. Kummer[2] K. Kliemt[3] C. Krellner[3] S. Seiro[4] C. Geibel[5] C. Laubschat,[1] Y. Kubo,[6] Y. Sakurai,[7] D. V. Vyalikh[8,9,†] and A. Koizumi[10]

[1]*Institut für Festkörper- und Materialphysik, Technische Universität Dresden, D-01069 Dresden, Germany*
[2]*European Synchrotron Radiation Facility, 71 Avenue des Martyrs, CS 40220, 38043 Grenoble Cedex 9, France*
[3]*Kristall- und Materiallabor, Physikalisches Institut, Goethe-Universität Frankfurt, Max-von-Laue Straße 1, D-60438 Frankfurt am Main, Germany*
[4]*Leibniz Institute for Solid State and Materials Research, Helmholtzstrasse 20, IFW Dresden, D-01069 Dresden, Germany*
[5]*Max-Planck-Institut für Chemische Physik fester Stoffe, D-01187 Dresden, Germany*
[6]*Department of Physics, College of Humanities and Science, Nihon University, Tokyo 156-8550, Japan*
[7]*Japan Synchrotron Radiation Research Institute (JASRI), SPring-8, Hyogo 679-5198, Japan*
[8]*Donostia International Physics Center (DIPC), 20018 Donostia/San Sebastián, Basque Country, Spain*
[9]*IKERBASQUE, Basque Foundation for Science, 48013 Bilbao, Spain*
[10]*Graduate School of Material Science, University of Hyogo, Hyogo 678-1297, Japan*

(Received 30 July 2020; revised 17 December 2020; accepted 21 January 2021; published 15 March 2021)

With the breakdown of coherent Kondo scattering with rising temperature, the Fermi surface (FS) in rare-earth Kondo lattices is expected to transition from the *large* FS counting the $4f$ moments, which form entangled quasiparticles with strongly enhanced effective masses with the conduction states, to the *small* FS with decoupled and localized $4f$ moments. A direct observation of this transition with temperature has, however, remained elusive, because conventional probes of the FS in Kondo lattices require high magnetic fields, which might reconstruct the FS or cannot work reliably at elevated temperatures. Using high-resolution Compton scattering, we overcome these limitations and show that the FS topology in the prototypical Kondo lattice $YbRh_2Si_2$ undergoes pronounced changes between 14 and 300 K in zero magnetic field. In particular, we present clear evidence for a largely restored small FS at room temperature. Our results suggest the relevant energy scale of the complex Kondo crossover phenomenon in $YbRh_2Si_2$.

DOI: 10.1103/PhysRevB.103.115126

I. INTRODUCTION

Rare-earth Kondo lattices belong to the most fundamental examples of strongly correlated electron systems. With a wealth of intriguing phenomena ranging from heavy-fermion behavior, competing exotic order, quantum criticality to unconventional superconductivity, they offer an inexhaustible playground to explore and model correlated states of matter [1–8]. Common to most of these systems is the central role of the rare-earth f orbitals, which reside in a paramagnetic lattice of localized moments at high temperatures and gradually start to couple to the itinerant valence states upon cooling. In a heavy-fermion Kondo lattice, the quenched f moments hybridize with the itinerant states and form heavy quasiparticle bands with strongly renormalized masses. The f-moment hybridization has a huge impact on the topology, volume, and effective mass of the Fermi surface (FS) and strongly determines the exotic transport properties in Kondo lattices. The central question arises, how the interactions between the itinerant states and the localized f-orbital moments affect the FS and what is the relevant energy and temperature scale, where these interactions come into play.

According to Luttinger's sum rule, the FS volume should accommodate the additional local f moment in the strong-coupling limit, when it is quenched by the Kondo screening and couples to the conduction bands [9,10]. This accommodation is realized by the formation of dispersive heavy quasiparticle bands at the Fermi level and the crossover from a *small* to a *large* FS. Conversely, the f moment should be released from the Fermi volume in the weak-coupling limit at elevated temperatures restoring the *small* FS. In spite of the general acceptance of this concept, clear experimental evidence of how and at which temperature scale the f-electron degrees of freedom decouple from the Fermi surface, is still lacking up to now for any Kondo lattice material. Numerous evidence has been found for a small-to-large Fermi surface transition in mostly Ce-based Kondo lattices at very low temperatures as a function of pressure or magnetic field, although some of these findings had to be reconsidered as Lifshitz transitions due to Zeeman splitting [11–15]. At the same time, no such transition as a function of temperature could be clearly traced to date experimentally. However, the formation of composite quasiparticles and the related temperature and energy scales is at the core of the physics of strongly correlated materials in general and Kondo and heavy-fermion systems in particular. It is especially noticeable that the emergence of the bound states between localized moments and conduction electrons in Kondo lattices shows a strong analogy to the

*Corresponding author: monika.guettler@tu-dresden.de
†denis.vyalikh@dipc.org

formation of Cooper pairs in superconductors [16,17]. But while the emergence of superconductivity with temperature and its implications for the Fermi surface has been exhaustively studied, the formation of the composite quasiparticles in Kondo lattices starting from independent localized moments at high temperatures and the emergence of the heavy-fermion state is yet poorly understood and experimental insight is notably scarce.

Until now, only few and indirect experimental evidence of a temperature-driven FS transition in Kondo lattices could be obtained [18–22]. There are two examples of a direct observation of the *large* FS by angle-resolved photoemission spectroscopy (ARPES) in $CeCoIn_5$ [22] and $YbRh_2Si_2$ [23,24]. For Ce-based heavy-fermion systems a transition from itinerant to localized f moments could be observed in the FS derived from high-resolution Compton profile measurements in $CeRu_2Si_2$ [25]. Yb-based heavy-fermion systems are the holelike equivalents to their Ce-based counterparts and as such should exhibit a similar itinerant-to-localized transition of the Yb $4f$ hole. However, Yb-based Kondo lattices are not as numerously studied as their Ce equivalents and no such observation could experimentally be made up to now in Yb systems. Here, we present evidence of a temperature-induced Kondo lattice crossover and the associated FS reconstruction in a prominent Yb-based Kondo lattice system, the prototypical heavy-fermion compound $YbRh_2Si_2$.

Recent ARPES results have revived the debate on the outstanding issue of the temperature scale, where the localized-to-itinerant crossover takes place [21,24]. While from thermopower and resistivity measurements [26] the local Kondo effect in $YbRh_2Si_2$ was found to set in around 80–100 K involving all crystal electric field (CEF) levels of the Yb^{3+} ions, tunneling spectroscopy [27] points to an onset of spatial coherence of the Kondo singlets at $T_L \approx 30$ K coinciding with the Kondo temperature T_K of the lowest ground-state CEF Kramers doublet. Unexpectedly, the spectral weight at the Fermi level probed by ARPES reflects a large FS even at a temperature of about 100 K, which is substantially higher than T_L [24]. Time-resolved ARPES showed that f-d hybridization in $YbRh_2Si_2$ persists even up to 250 K [28]. Likewise, Jang *et al.* report ARPES and dynamical mean field theory (DMFT) studies on $CeCoIn_5$ showing that f-spectral weight and enhancement of the effective mass survive at temperatures of at least ∼200 K [21], which is substantially higher than 45 K, where the onset of spatial coherence has been deduced from transport measurements. They suggest that the thermally populated higher CEF levels play a significant role in the formation of the Kondo lattice far above the transport coherence temperature. Furthermore, they point out that coherence develops not just at the resistivity maximum but already at higher temperatures, where deviations from the $-\ln T$ resistivity start to appear and then increase upon cooling. This would shift the expected onset of Kondo lattice coherence and thus the increase of the FS volume in $YbRh_2Si_2$ to temperatures around 200–300 K, i.e., well above ∼100 K where the resistivity maximum was observed [6,29]. The central question arises, at which temperature scale the crossover from the large to the small FS finally takes place.

Angle-resolved photoemission spectroscopy and the observation of quantum oscillations are the most common techniques to map the FS of a metallic system. However, these methods impose certain restrictions on the experimental conditions and the accessible phases of the material. Quantum oscillations require very low temperatures and high magnetic fields of several Tesla, but $YbRh_2Si_2$ is already driven through the quantum-critical point (QCP) at a small field of ∼60 mT [30]. Quantum oscillations are thus inherently not able to access the FS of $YbRh_2Si_2$ on the antiferromagnetic (AFM) side of the QCP and to explore its temperature evolution. ARPES, on the other hand, gives well resolved results only below temperatures of approximately 100 K due to thermal broadening effects.

A well suited and complementary method to derive the FS topology at zero field and room temperature is the measurement of high-resolution Compton profiles (HRCP) for the construction of the electron occupation number density (EOND) [25,31]. HRCP measurements are photon-in photon-out experiments employing high-energy photons of about 100 keV. Hence they give truly bulk-sensitive information on the electron momenta in the solid, which is in contrast to ARPES, for instance, where the short electron–mean free path is strongly limiting the probing depth. Furthermore, photoemission matrix element effects in ARPES may attenuate excitations from electronic states of certain symmetry and orbital character and thus give an incomplete picture of the FS. Compton scattering (CS), by contrast, probes *all* electrons on an equal footing giving a full account of the electron momentum density (EMD) in the sample, from which the shape of the FS can be derived. In a Kondo lattice like $YbRh_2Si_2$, the FS is defined by subtle hybridization of itinerant electrons with localized $4f$ moments. Any changes of the FS topology, which are attributed to the interplay of these two distinct sets of electronic states, should thus be detectable by CS, a method equally sensitive to all electrons.

In the present study we have performed HRCP measurements to visualize the evolution of the FS of $YbRh_2Si_2$ with temperature. As a reference, we have additionally carried out HRCP measurements on the well-studied compound $YbCo_2Si_2$ and compared the reconstructed EOND to *ab initio* band-structure calculations. Our experimental results show pronounced changes in the Fermi surface of $YbRh_2Si_2$ between 14 and 300 K. The persistence of the large Fermi surface in $YbRh_2Si_2$ up to temperatures of 100 K was previously demonstrated with ARPES [24]. In line with these earlier results we find that the EOND of $YbRh_2Si_2$ at 14 K strongly deviates from that of $YbCo_2Si_2$, the reference compound for the small Fermi surface. By contrast, going to room temperature the EOND of $YbRh_2Si_2$ strongly evolves now resembling that of $YbCo_2Si_2$. For the well-localized reference system $YbCo_2Si_2$ we observe no significant changes of the FS topology between 14 and 300 K in agreement with expectations. This long-sought direct observation of the temperature-driven Fermi surface reconstruction in $YbRh_2Si_2$, and in Yb Kondo lattices in general, sets a frame for the temperature scale of the reconstruction process and will help to further advance our theoretical understanding of the complex Kondo crossover phenomenon.

II. METHODS

The HRCP measurements were performed on beamline BL08W at the SPring-8 synchrotron in Japan on high-quality

$YbRh_2Si_2$ and $YbCo_2Si_2$ single crystals [32,33]. We used linearly polarized x-rays of 115.56 keV energy and set the scattering angle to about 165.5°. The Compton-scattered x-rays were resolved energetically with a Si(620) bent crystal analyzer and detected by a position-sensitive detector, which combines an image intensifier with a CCD camera. The analyzer and detector were arranged on the same Rowland circle.

Each Compton profile in an HRCP measurement results from a Compton-shifted line, which is broadened by the Doppler effect due to the motion of the electrons along the scattering direction. From the Doppler broadening, the momentum density of the electrons in the crystal can be derived. As each HRCP reflects the EMD projected onto a single line along the scattering vector, a series of measurements along equally spaced directions is required to reconstruct the EMD. The EMD essentially represents the momentum density in the extended zone scheme. It can be transformed into the electron occupation number density by folding all higher-momentum components into the first Brillouin zone [34]. The EOND integrates over all occupied states in the first BZ and as such undergoes its most pronounced changes at discontinuities in the transition from occupied to unoccupied states, i.e., at the FS. CS is thus the method of choice to probe the bulk FS of single crystals at conditions not accessible by common fermiology techniques such as ARPES or quantum oscillations.

To reconstruct the two-dimensional (2D) EMD, five directional Compton profiles were measured at evenly spaced intervals from the [100] to the [110] axes. Each HRCP was collected for 20 h. The measured HRCPs were carefully corrected for scattering cross section, background, multiple scattering, and x-ray absorption in the sample. X-ray fluorescence from a mixture of Bi and Tl was used for energy calibration. The fluorescence lines were corrected for CCD image distortion. The energy scale was converted to the momentum scale with a momentum resolution of 0.096 (0.113) a.u. full width at half maximum for $YbRh_2Si_2$ ($YbCo_2Si_2$) determined by the energy resolution of the spectrometer and monochromator and by the angular resolution. Prior to reconstructing the momentum density, each HRCP was normalized by the electron number within the measured momentum range, which was estimated by using Hartree-Fock profiles. From the five normalized HRCPs, the 2D EMD was reconstructed using the direct Fourier-transform method [35,36] and expanded according to the crystal symmetry. Finally, the EOND obtained by Lock-Crisp-West folding [34] was projected onto the k_x-k_y plane resulting in the projection of the Fermi volume from all contributing FSs onto a grid of 23 × 23 **k** points within the first 2D BZ.

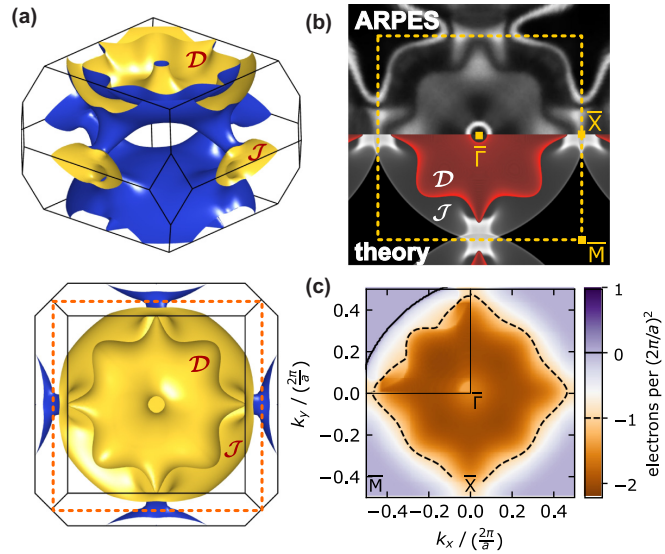

FIG. 1. Fermi surface of $YbCo_2Si_2$. (a) Three-dimensional representation of the calculated FS. The blue and yellow sides point towards occupied and unoccupied states, respectively. Consequently, $\mathcal{D}$ is a hole surface and $\mathcal{J}$ a largely interconnected sheet. The square marked by the dashed line indicates the projected 2D BZ. (b) Upper half: projected FS obtained by ARPES from a Si-terminated crystal [39]. Lighter shades correspond to higher photoemission intensity. Lower half: theoretical projected FS from a pure bulk calculation corresponding to the FS in (a). The $\mathcal{D}$ FS sheet is highlighted in red. (c) Calculated EOND for $YbCo_2Si_2$ projected onto the k_x-k_y plane. Except for the upper left quadrant, the 2D-EOND has been convoluted with the experimental resolution of 0.13 $\frac{2\pi}{a}$ full width at half maximum. The color scale denotes the number of electrons (holes) per $(\frac{2\pi}{a})^2$. The integral of the EOND over the projected BZ, which reflects the FS volume, adds up to one hole. The solid and dashed contour lines mark the levels of −0.01 (just below the maximum value of the plateau) and −1 electrons (+1 holes) per $(\frac{2\pi}{a})^2$.

III. RESULTS

A. *Small* Fermi surface in $YbCo_2Si_2$

$YbCo_2Si_2$ is isostructural and isoelectronic to $YbRh_2Si_2$. Residing far on the AFM side of the QCP in the Doniach phase diagram, the onset of AFM order ($T_N = 1.7$ K) outruns the rather weak Kondo effect ($T_K < 1$ K) [33]. Although signatures of weak $4f$ hybridization show up at lowest temperatures, they do not lead to a coherent Kondo lattice formation with renormalized heavy quasiparticle bands leaving the FS small [37–39]. Therefore, $YbCo_2Si_2$ is an ideal reference system for a comparison with $YbRh_2Si_2$, with well-localized $4f$ electrons without sizable Kondo interaction [40].

Before we start the discussion with our theoretical and experimental results on the reference compound $YbCo_2Si_2$, it is helpful to recall the topology of its bulk FS, which has already been published earlier [39] and is shown in Fig. 1(a). The electronic structure of this material was calculated within density functional theory (DFT) in the generalized-gradient approximation using a full-potential local-orbital code [41]. To account for the well-localized paramagnetic $4f$ moments, we used a fixed, nonmagnetic $4f^{13}$ configuration within a frozen-core approximation. In our calculation, the FS is formed by two distinct bands: the doughnut $\mathcal{D}$, a large hole pocket centered around the Z point in the bulk Brillouin zone (BZ), and the jungle-gym $\mathcal{J}$, a largely interconnected sheet across the whole **k** space. Depending on the employed z_{Si} parameter for the Si atoms, an additional, small electron pocket around Γ, the so-called pillbox $\mathcal{P}$, can be present [42]. In our band-structure calculations we used the Wyckoff position

component $z_{Si} = 0.379$, for which the band forming the pillbox is pushed above the Fermi level and does not contribute to the Fermi surface. This value for the z_{Si} parameter is motivated by the results of previous quantum oscillation experiments and single crystal structure refinement [43] and, as shown below, also yields the best agreement with our experimental results. In Fig. 1(b), a previously obtained UV-ARPES map of the FS measured from a Si-terminated crystal at 10 K is depicted for reference and compared to the projection of the calculated bulk FS along k_z, the crystal momentum component parallel to the surface normal [39].

The frozen-core approach proved to lead to a perfect agreement between the calculated and ARPES-derived electronic structure of the valence bands, as can be seen in Fig. 1(b). Note that we projected the pure bulk FS in the lower part of the panel omitting any surface-related states. Thus the sharp diamond-shaped band within the projected gap around the $\overline{M}$ point in the ARPES results, which has been shown to be a Shockley surface state [39,44,45], is not reproduced in the calculation. Furthermore, the ARPES experiment could not verify whether the pillbox $\mathcal{P}$ is part of the FS at $\overline{\Gamma}$ or not, because this region is masked by a strong surface resonance giving rise to the bright ring-shaped intensity around $\overline{\Gamma}$ in the ARPES map. Apart from these two surface-related states, the calculated bulk FS agrees remarkably well with the FS obtained by ARPES. As hybridization of the purely *spd*-derived valence band with the frozen $4f$ core states is suppressed in our calculation, the FS does not count the localized $4f$ hole and is consequently *small*. The ARPES experiments thus demonstrated the existence of the small FS with a localized $4f$ moment in $YbCo_2Si_2$. The band-structure calculation clearly traces the topology and size of the FS of $YbCo_2Si_2$ with high accuracy and can be used as a reliable starting point for the calculation of its EOND.

In Fig. 1(c) we show the calculated EOND of paramagnetic $YbCo_2Si_2$. The band-structure calculation used for the construction of the EOND is the same as the one underlying the projected FS in Fig. 1(b). The EOND sums up all occupied states from the two contributing FS sheets. With a trivalent Yb ion $YbCo_2Si_2$ is an uncompensated metal, i.e., the electron and hole contributions to the Fermi surface do not add up to zero. The holelike character of the doughnut $\mathcal{D}$ and the jungle-gym $\mathcal{J}$ is evident from the total number of occupied states contained in each band, which amount to 1.75 for $\mathcal{D}$ and 1.23 for $\mathcal{J}$, summing up to a total FS volume of one hole [46]. These numbers are in perfect agreement with the values obtained in Ref. [47] for $YbRh_2Si_2$ with localized $4f$ states. The theoretical EOND in Fig. 1(c) shows a large area of unoccupied states with increasing negative contribution towards the BZ center from both $\mathcal{D}$ and $\mathcal{J}$ and a small circle of elevated electron occupation at $\overline{\Gamma}$ from the topological hole in $\mathcal{D}$. The integral of the calculated EOND over the projected BZ corresponds to the FS volume and amounts to one hole or -1 electrons. The electron density reaches a maximum plateau around the $\overline{M}$ point, where it vanishes, as no bands cross the Fermi level in this region. As the calculated electronic structure has already proven to be in good agreement with the ARPES results, the calculated EOND can reasonably be assumed to be a valid reference for the EOND of the *small* FS.

B. EOND in $YbCo_2Si_2$ at low and room temperature

From the measured HRCPs of $YbCo_2Si_2$ and $YbRh_2Si_2$ we reconstructed the EONDs at 300 and 14 K as described in the Methods section. The lower temperature is sufficiently below the single-ion Kondo temperature of the CEF ground state in $YbRh_2Si_2$ and the observed onset of spatial coherence in tunneling spectroscopy [27], which are both about 30 K. The experimental results are depicted in Fig. 2. Note that the experimentally obtained EONDs include a large isotropic background from Compton scattering by core electrons and valence electrons from fully occupied bands [48]. Due to the different number of total electrons per unit cell, this background contribution is different for $YbCo_2Si_2$ and $YbRh_2Si_2$. In Fig. 2 we account for this background and thus make the EONDs of the two systems comparable by showing them with respect to the experimentally observed mean electron density for each compound, which is independent of the temperature.

The EONDs of $YbCo_2Si_2$ at 300 and 14 K in Fig. 2, left column, are very similar and, apart from a constant offset, in good agreement with the theoretical EOND in Fig. 1(c). The experimental EONDs are dominated by two contributions. The first contribution can be found in the corners of the projected BZ, where mostly occupied states pile up. These fully occupied parts are well reproduced in the calculation. The large, light diamond centered around the $\overline{\Gamma}$ point and reaching up to the $\overline{X}$ points can be attributed to the cumulated holelike contributions of the doughnut $\mathcal{D}$ and the jungle-gym $\mathcal{J}$. A more quantitative comparison with the calculated EOND can be achieved, when the isotropic contributions from fully occupied bands and core levels are removed from the experimental EOND. To this end, we removed a constant offset from the experimental EONDs of $YbCo_2Si_2$ such that the integrated EOND adds up to one hole, i.e., the same value is in the calculations. The resulting EONDs are shown in the left column of Fig. 3. With this normalization, the similarity between the experimental EOND map of $YbCo_2Si_2$ at 14 K and the calculation in Fig. 1(c) becomes more evident due to the matching electron density scales. An important observation is, that the $YbCo_2Si_2$ EOND does not significantly change upon increasing the temperature to 300 K and essentially retains its shape corresponding to the underlying small FS. The slight changes in electron density observed between 14 and 300 K are within the experimental uncertainties.

There could be some physical reasons why the CS response in $YbCo_2Si_2$ may not exactly be the same at low and room temperature. In a previous resonant x-ray emission spectroscopy experiment [49] minute changes in the Yb valence between low and room temperature even in the nominally stable trivalent $YbCo_2Si_2$ were observed, which were about a factor of 10 smaller than, for instance, in $YbRh_2Si_2$. Hence it is possible that even the FS in $YbCo_2Si_2$ shows very small changes from low to room temperature. A second aspect is that at room temperature the FS is not a well-defined concept anymore. The separation between occupied and unoccupied states is washed out by about 4 k_BT, which should have a small effect on the CS profiles. The important point is, however, that if there are differences in the low- and high-temperature EOND of $YbCo_2Si_2$, they are only very

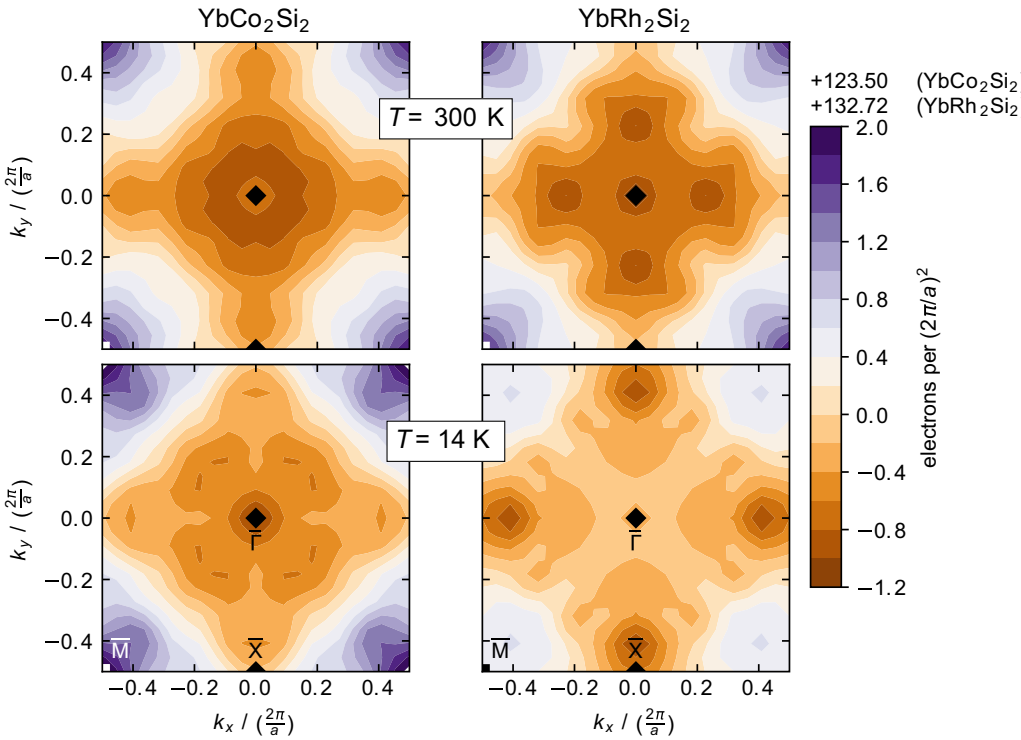

FIG. 2. Projected experimental 2D EOND of $YbCo_2Si_2$ and $YbRh_2Si_2$ at 300 and 14 K. Each EOND map has been reconstructed from five directional HRCPs as described in the Methods section. To ease comparison between the two systems the maps are shown with respect to the mean electron density indicated above the colorbar for both compounds.

small demonstrating an essentially temperature-independent situation. We will show that $YbRh_2Si_2$ behaves very differently and displays a strongly changing EOND between 14 and 300 K.

In Fig. 4, we show the cut along $\overline{M}$-$\overline{\Gamma}$-$\overline{X}$ for all EOND maps normalized to both the mean electron densities and to the Fermi volumes, which corresponds to the display in Figs. 2 and 3, respectively. A calculated EOND profile of $YbCo_2Si_2$ broadened with the experimental resolution is added for comparison. We note that the shape of the calculated profiles around $\overline{\Gamma}$ and $\overline{X}$ varies with z_{Si} and that best agreement between theory and experiment can be obtained for $z_{Si} = 0.379$. In the Supplemental Material [50] we compare the experimental data to a range of calculated profiles obtained for different positions z_{Si} of the Si atom within the unit cell.

The profiles for $YbCo_2Si_2$ at both temperatures show very similar shapes within our experimental accuracy and also agree qualitatively well with the calculated profile except around the high-symmetry points $\overline{M}$ and $\overline{\Gamma}$. In the calculation the EOND around $\overline{M}$ has a flat plateau indicating constant electron occupation with no bands crossing the Fermi level along k_z, whereas the measured EOND immediately drops with an almost constant slope from $\overline{M}$ towards $\overline{\Gamma}$. This deviation around $\overline{M}$ might be caused by residual overshooting effects due to the band limitation in the reconstruction algorithm (see Supplemental Material [51]). Around the $\overline{\Gamma}$ point, only the 300 K EOND of $YbCo_2Si_2$ agrees well with the calculation. However, from error maps of the reconstructed EONDs shown in the Supplemental Material [51] it is evident that the experimental error is typically largest around the BZ origin. We therefore conclude that the agreement between the experimental and calculated EOND profiles for $YbCo_2Si_2$ is reasonably good.

To summarize, according to our CS experiment, the FS of $YbCo_2Si_2$ does not change in shape and volume from 300 K to the lowest measured temperature of 14 K. From the temperature independence of the experimental EOND and its similarity to the calculated EOND, we conclude that our CS experiment detects a stable, *small* FS in $YbCo_2Si_2$ at low and room temperature, in agreement with previous low-temperature ARPES results [39].

C. EOND in $YbRh_2Si_2$ at low and room temperature

From our data on $YbCo_2Si_2$ we have established the shape of the EOND, which can be expected for the *small* FS. We now turn to the CS results for $YbRh_2Si_2$, which were obtained in exactly the same way as for $YbCo_2Si_2$. The two resulting EONDs normalized to the mean electron density are shown in the right column of Fig. 2. Comparing the EOND at 14 K with the 300 K result, the EOND and thus the FS in $YbRh_2Si_2$ appears to undergo drastic changes between these two temperatures. We stress again that at $T = 14$ K we are sufficiently below the single-ion Kondo temperature of the lowest lying Kramers doublet and the transport coherence temperature $T_L \approx 30$ K, where the Kondo lattice formation should be well established. At room temperature we are well above this regime ($T \approx 10T_L$).

Starting at 14 K, the $YbRh_2Si_2$ EOND considerably deviates from that of $YbCo_2Si_2$ in Fig. 2. First, the width of the bright diamond shape formed by negative electron density becomes notably larger around the $\overline{X}$ points, with broad necks

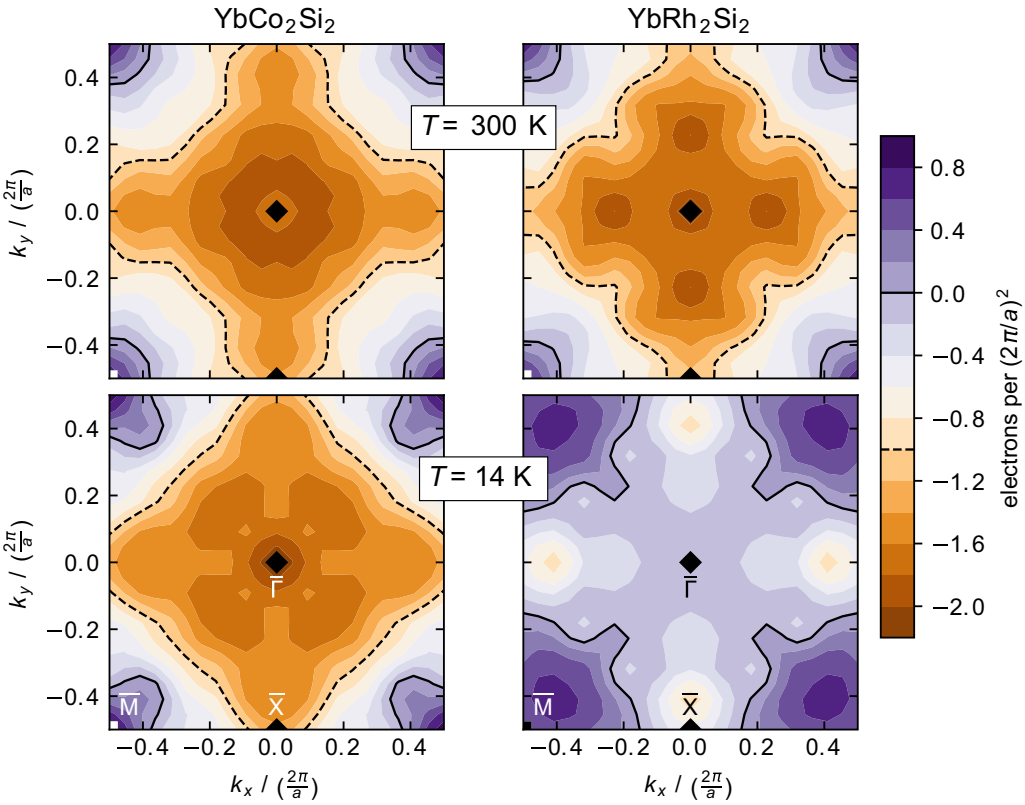

FIG. 3. Projected experimental 2D EOND of $YbCo_2Si_2$ and $YbRh_2Si_2$ at 300 and 14 K normalized to the expected Fermi volume. For $YbCo_2Si_2$ (300 and 14 K) and $YbRh_2Si_2$ at 300 K the zero level is set to result in an integrated value of -1 electrons, i.e., one hole. The large FS of $YbRh_2Si_2$ at 14 K is known to be nearly compensated and the zero level of the EOND is, therefore, set to give an integrated value of zero. In all EOND maps, solid and dashed lines trace the 0 and -1 electrons per $(\frac{2\pi}{a})^2$ contours.

opening at the BZ border. From a qualitative comparison with the calculated small FS of $YbCo_2Si_2$, one can expect these necks to arise from both the $\mathcal{D}$ and the $\mathcal{J}$ EOND (compare Fig. S2 in the Supplemental Material [52]), as the unoccupied parts of the electron density increase in size and extend towards the second Brillouin zone. This observation is in line with the open necks in the $\mathcal{D}$ sheet of the large FS of $YbRh_2Si_2$ seen by ARPES up to 100 K [24]. A striking difference in the $YbRh_2Si_2$ EOND at 14 K compared to $YbCo_2Si_2$ is a strong reduction of electron density close to the $\overline{M}$ points, while it increases in the BZ center. It appears as if electron density is redistributed from the $\overline{M}$ and $\overline{X}$ points towards the center, which results in an overall flattening of the EOND across the entire projected BZ. These effects are even more evident in the EOND profiles shown in Fig. 4(a).

Upon raising the temperature to 300 K, the EOND in Fig. 2 strongly changes and resembles qualitatively the experimental result obtained for $YbCo_2Si_2$. Both the size and overall shape of the diamond structure as well as the strongly occupied corners of the projected BZ are in good qualitative agreement with the EOND seen in $YbCo_2Si_2$. The absolute values of the electron densities normalized to the mean values are in remarkable agreement as well. This is also evident from a comparison of the EOND profiles in Fig. 4(a). Consequently, the $YbRh_2Si_2$ EOND at 300 K also shows good qualitative agreement with the small-FS EOND calculated for $YbCo_2Si_2$ [Fig. 1(c)]. Note, that for a hypothetical small FS in $YbRh_2Si_2$ the calculated EOND would be virtually identical to that of $YbCo_2Si_2$ (see Supplemental Material [53]).

From Fig. 4(a), a minor difference between the EONDs of $YbRh_2Si_2$ at 300 K and of $YbCo_2Si_2$ is evident in the presence of an additional dip in the $YbRh_2Si_2$ EOND halfway between $\overline{\Gamma}$ and $\overline{X}$. A similar dip can be found in the EOND profile of $YbRh_2Si_2$ at 14 K around $0.4\,2\pi/a$ along $\overline{\Gamma}$-$\overline{X}$. These dips might therefore be related to each other by having a similar origin in the Fermi surface. However, their amplitude barely exceeds the propagated statistical error of the experiment. We discuss this feature in more detail in the Supplemental Material [54].

Hall effect measurements combined with renormalized band-structure calculations on $YbRh_2Si_2$ have shown that the holelike contributions from the doughnut and the electronlike contributions from the jungle-gym FS sheets nearly compensate each other in the Kondo lattice regime [47]. This result reflects the working of the Luttinger theorem, which requires the hybridizing $4f$ moment to be counted in the Fermi volume. Starting from a prototypical small FS such as the one of $YbCo_2Si_2$ with one hole, the additional $4f$ hole gives a count of two modulo the BZ volume resulting in an effectively compensated FS with a total Fermi volume of zero. We thus know that the integrated EOND of $YbRh_2Si_2$ at low temperatures should sum up to zero. In Fig. 3, we therefore show the experimental EOND of $YbRh_2Si_2$ at 14 K after subtraction of its mean value, i.e., such that its integral over the BZ is

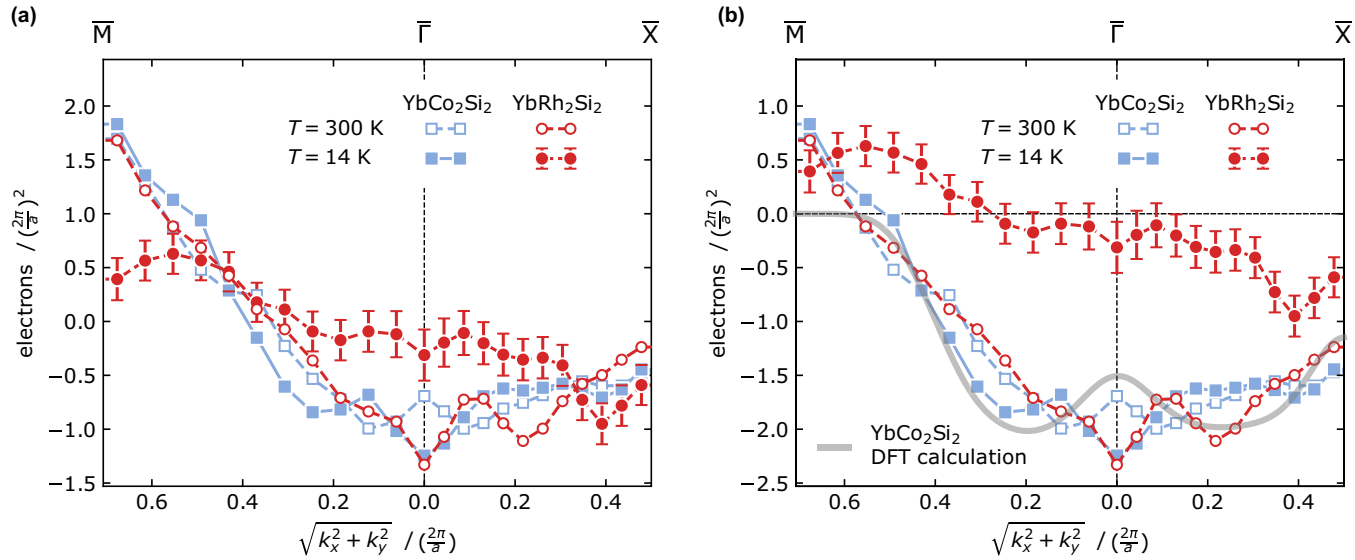

FIG. 4. EOND cuts along $\overline{M}$-$\overline{\Gamma}$-$\overline{X}$ for $YbCo_2Si_2$ and $YbRh_2Si_2$ at 300 and 14 K. In (a), the EOND is normalized to the mean electron density. In (b), the same **k**-independent offset has been subtracted as in Fig. 3, i.e., for $YbCo_2Si_2$ (300 and 14 K) and $YbRh_2Si_2$ at 300 K the zero level is set to result in an integrated value of -1 electrons, i.e., one hole. For $YbRh_2Si_2$ at 14 K, the EOND is normalized to add up to zero electrons. The errorbars have been estimated by propagating the statistical error of ± 0.2–0.3% in the Compton profiles through the reconstruction and Lock-Crisp-West folding. For clarity we only show errorbars for one curve, as they are very similar for all EONDs. The gray solid line shows the profile through the calculated EOND for $YbCo_2Si_2$ after broadening with the experimental resolution.

zero. Having also established that $YbCo_2Si_2$ has an uncompensated FS with a volume of one hole, we are only left with an unknown FS volume of $YbRh_2Si_2$ at 300 K. The strong resemblance of the $YbRh_2Si_2$ EOND at 300 K to $YbCo_2Si_2$ in Figs. 2 and 4(a) strongly indicates a close similarity of the underlying Fermi surfaces and that the high-temperature FS of $YbRh_2Si_2$ is no longer compensated. In Fig. 3 we therefore show the experimental EOND of $YbRh_2Si_2$ at 300 K after subtraction of a constant, **k**-independent offset chosen such that the integral over the EOND, and thus the Fermi volume, is equal to one hole, as in the case of $YbCo_2Si_2$ (see Supplemental Material [55]). One can see immediately the good quantitative agreement between the high-temperature EOND of $YbRh_2Si_2$ and the EOND of $YbCo_2Si_2$. Moreover, the EOND profile of $YbRh_2Si_2$ at 300 K in Fig. 4(b) reasonably matches the profiles of $YbCo_2Si_2$ within the experimental accuracy, which was already evident in the data referred to the mean electron number in Fig. 4(a).

In essence, when moving from 300 to 14 K, the representation of the $YbRh_2Si_2$ EOND as shown in Figs. 2 and 4(a) reveals a presumably even redistribution of electron density mostly from the $\overline{M}$ points over the whole Brillouin zone. A hand-waving argument might be that the formation of the composite quasiparticles with the localized $4f$ electrons effectively binds an itinerant conduction electron per unit cell and suppresses its **k** dependence. This would naturally lead to a change in the Fermi volume, and thus the integrated value of the **k**-dependent EOND, upon entering the Kondo regime, as shown in the data representation in Figs. 3 and 4(b). At the same time, the integral of the total experimental EONDs remains invariant [Figs. 2 and 4(a)], as the total number of electrons in the system does not change. The difference between the two representations is that the EONDs in Figs. 3 and 4(b) reflect the carrier types contributing to the Fermi surface. Figure 3 would thus illustrate a transition upon cooling from a mostly holelike, *small* Fermi surface to a compensated, *large* FS with equal electron- and holelike contributions as indicated by renormalized band-structure calculations [47].

IV. DISCUSSION

To answer the question whether and how the FS of $YbRh_2Si_2$ changes with temperature, we needed a reference of a similar compound with well understood *small* FS. We have obtained the electron occupation number density of $YbCo_2Si_2$ both by means of Compton scattering for low and room temperature and DFT calculations and found a qualitatively good agreement among all EONDs. The calculated EOND originates from nearly the same band-structure calculation as the one which already gave a nice agreement with an ARPES mapping of the FS [39]. Our results confirm the existence of the small FS in $YbCo_2Si_2$ and show no significant temperature evolution between 14 and 300 K.

In contrast, the EOND of $YbRh_2Si_2$ shows a dramatically different behavior. At 14 K, the $YbRh_2Si_2$ EOND considerably deviates from that of $YbCo_2Si_2$ and shows a notable redistribution of electron density from the BZ borders towards the center. While the electron density increases around $\overline{\Gamma}$, it is depleted with increasing **k** vector around $\overline{M}$ and $\overline{X}$, which results in an overall flattening of the EOND. From previous ARPES experiments it is known that the Fermi surface of $YbRh_2Si_2$ is *large* at least below 100 K. These profound differences between the low-temperature EOND of $YbRh_2Si_2$ and the EOND of $YbCo_2Si_2$, the *small* FS reference, can therefore be attributed to signatures of the reconstructed, *large* FS found in $YbRh_2Si_2$ at 14 K.

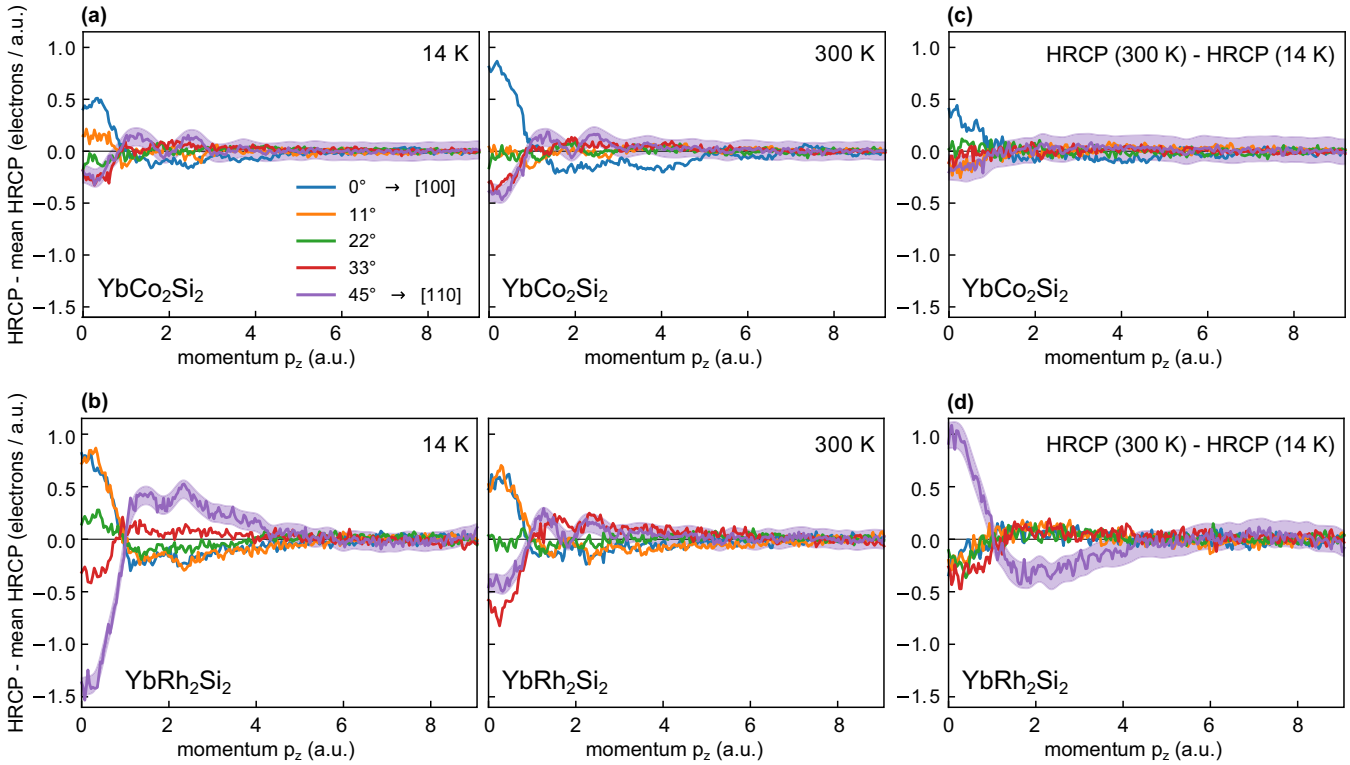

FIG. 5. Directional Compton profiles of (a) $YbCo_2Si_2$ and (b) $YbRh_2Si_2$ for 14 K (left) and 300 K (right) after subtracting the average over all five profiles for each compound and temperature. The five Compton profiles were taken along five evenly distributed directions between 0° and 45° relative to the [100] direction in the 2D k_x- k_y plane. (c),(d) Difference for each direction between the profiles taken at 300 and 14 K for (c) $YbCo_2Si_2$ and (d) $YbRh_2Si_2$.

A detailed derivation of the large FS topology of $YbRh_2Si_2$ at low temperature from the CS data is limited by the contribution of several overlapping FS sheets, the projection of the EOND on a two-dimensional subspace, and the limited momentum resolution of the method. It is therefore beyond the scope of this work. Nevertheless, we would like to make a few qualitative remarks to complement the insights obtained from other experiments. What is quite evident is that an enlargement of the $\mathcal{D}$ FS alone cannot explain the observed changes in the experimental EONDs. The shape of the $\mathcal{D}$ sheet in both the large and the small FS is well known from ARPES studies [23,39]. In either case, this FS sheet does not come close to the $\overline{M}$ points and therefore cannot account for the strong EOND changes around the BZ corners. The dramatic changes around the $\overline{M}$ point of the projected BZ suggest a strong participation also of the more extended $\mathcal{J}$ FS sheet in the FS reconstruction from *small* to *large*. Interestingly, the jungle-gym at low temperature could not clearly be traced in ARPES [23]. Similarly, quantum oscillation experiments could not observe frequencies of the $\mathcal{J}$ sheet or attributed frequencies to $\mathcal{J}$ that strongly deviated from LDA predictions [12,43,56]. Our band-structure calculations have found that both FS sheets, $\mathcal{D}$ and $\mathcal{J}$, are composed of Si $3p$ and Rh $4d$ orbitals with similar ratios in the high-temperature $4f$-localized phase. Therefore it is reasonable to assume that both sheets are similarly prone to f-d hybridization and the holelike $\mathcal{J}$ volume should simultaneously increase to $\mathcal{D}$. As the $\mathcal{J}$ band crosses the Fermi level already quite close to the projected BZ border, the electronlike renormalized bands might be partly pushed above the Fermi level in the **k** space projected onto the $\overline{M}$ points. Such a scenario is schematically illustrated in the Supplemental Material [57].

The central finding of this work is a strong change of the $YbRh_2Si_2$ EOND upon heating from 14 to 300 K, in stark contrast to a temperature-independent EOND in $YbCo_2Si_2$. A strong temperature effect for $YbRh_2Si_2$ is likewise observable already in the raw directional Compton profiles, as shown in Fig. 5. The figure shows the Compton profiles for both $YbCo_2Si_2$ and $YbRh_2Si_2$ at 14 and 300 K for the five directions of the scattering vector after subtraction of the average over all profiles for each compound and temperature. From a qualitative comparison of the Compton profiles between both compounds and especially from the temperature-difference profiles [panels (c) and (d)] it is immediately evident that the Compton scattering response for $YbRh_2Si_2$ differs significantly stronger between 300 and 14 K than for $YbCo_2Si_2$. At 300 K, the directional profiles of $YbRh_2Si_2$ get much closer to those of $YbCo_2Si_2$ than at 14 K. The difference profiles with temperature for $YbRh_2Si_2$ show a strong anisotropy with notable weight transfer even beyond the first Brillouin zone, which cannot be directly attributed to changes in the coherent band structure constituting the Fermi surface. This electronic weight is inseparably connected to the formation of the composite quasiparticles with increasing f-d hybridization at low temperature. As discussed earlier, the entanglement of the

conduction electrons with the localized f moments leads to an *effective* localization of one electron per Yb site, which in turn has to be drawn from the Fermi volume. This involves extensive correlations in momentum space with an anisotropic signature reflecting the anisotropic f-d hybridization, which results in an increased anisotropy in the high-momentum contributions to the electron momentum density and thus to an increased anisotropy in the Compton profiles.

From a comparison of the reconstructed EMDs at 300 and 14 K in $YbRh_2Si_2$ we found a slight reduction in the integrated electron density up to 0.8 a.u. of about 0.06 ± 0.04 electrons per formula unit at low temperature compared to the high-temperature EMD. The upper bound of 0.8 a.u. equals the distance between the first and second $\overline{\Gamma}$ points. As the total number of electrons must remain constant, the missing electron density has to be distributed over larger momenta. However, as the valence electrons mainly contribute to small momenta and localized electrons are spread in momentum space over a broad range of larger momenta, this fraction of electrons flowing from small to larger momenta roughly points to a spatial localization of these electrons. In contrast, we have found that the corresponding change in electron density in $YbCo_2Si_2$ lies, as expected, within the range of the statistical error.

These numbers have to be taken cautiously as (i) the reconstructed two-dimensional EMDs still contain the integrated contributions along the p_z axis, and (ii) the upper bound of 0.8 a.u. is certainly chosen somewhat arbitrarily. Nevertheless, our result on $YbRh_2Si_2$ is in good agreement with the valence change in $YbRh_2Si_2$ with temperature observed by resonant x-ray emission spectroscopy [24], which was found to be less than 0.05 per Yb ion between 300 and 1 K. It might seem surprising that the number of localizing electrons—or equivalently delocalizing holes—in $YbRh_2Si_2$ is much smaller than one. However, our present findings are in line with the notion that the huge change in the Fermi surface volume is not rooted in valence fluctuations but rather in the fulfillment of the Luttinger sum rule due to the onset of the f-d hybridization, which requires the $4f$ hole to be counted in the Fermi surface, while it remains nearly localized even at low temperatures [58].

From the qualitative analysis of the Compton profiles and from the closeness of the high-temperature EOND of $YbRh_2Si_2$ to the experimental and calculated EONDs of $YbCo_2Si_2$, we conclude that the underlying FS of $YbRh_2Si_2$ at 300 K is comparable to the well-established, *small* FS of $YbCo_2Si_2$ with well-localized f electrons. Going from 14 to 300 K the single-particle excitations in $YbRh_2Si_2$ therefore seem to evolve as predicted by the Kondo lattice model, i.e., in line with the anticipated crossover from the *large* towards the *small* FS topology.

The observation that the Fermi surface in $YbRh_2Si_2$ is still the large one at a temperature T of 100 K [24], far above the Kondo temperature of the ground-state doublet and above the onset of coherence seen in the T dependence of the resistivity, intensified the debate on the appropriate description of the emergence of coherence in Kondo lattices, on the renormalization of the FS, and on the relevant temperature scales. The recent pump-probe ARPES study on $YbRh_2Si_2$ of Leuenberger *et al.* [28] provides clear evidence that the dehybridization of the f electrons takes place in the T range between 100 and at least 250 K. A similar dehybridization temperature scale was also observed using T-dependent ARPES in the Kondo lattice $CeCoIn_5$ [21]. In addition, Ref. [21] shows that such a large dehybridization T scale is in good agreement with theoretical predictions from DMFT calculations. However, neither [28] nor [21] could specify in which way the FS was affected. The present results clearly show that at 300 K the FS of $YbRh_2Si_2$ has largely transformed to the small FS, i.e., to the dehybridized one. Thus combining the present results with those of Refs. [24] and [28], one can safely conclude that the dehybridization of the $4f$ electrons is connected with a change from the large to the small FS. This change occurs in a continuous process mostly in the T range $100\ \mathrm{K} < T < 300\ \mathrm{K}$, in accordance with general predictions of DMFT calculations [59].

The T scale $100\ \mathrm{K} < T < 300\ \mathrm{K}$ for the dehybridization process implied by the present results and Refs. [21,28] is larger than all temperature scales proposed as Kondo or coherence scale derived from other types of measurements as, e.g., transport or specific heat. Specifically the present Compton and recent ARPES results provide a clear indication that in Kondo lattice systems the hybridization of the $4f$ and valence states starts very far above the onset of coherence observed in the T dependence of the resistivity $\rho(T)$. Moreover, the reconstruction of the large FS is almost completed at the onset of this coherence. At first sight such a large difference in "coherence" temperatures might look surprising and inconsistent, but as we discuss in detail in the Supplemental Material [60], this apparent inconsistency in energy scales is just a consequence that the "coherence" effects seen in resistivity and in ARPES and Compton measurements correspond to different phenomena [24]: The formation of a larger FS as seen in ARPES and Compton scattering relies on the $4f$'s spectral function acquiring momentum dependence due to hybridization with dispersive conduction states. In contrast the onset of coherence effects in $\rho(T)$ relies on the disappearance of inelastic scattering connected with the lattice Kondo effect. One expects the latter process to occur at temperatures below the T scale of the former process. Similarly, further energy scales deduced from other types of measurements also correspond to distinct underlying mechanisms (see Supplemental Material [60]).

In summary, we have obtained the electron occupation number densities from high-resolution Compton profiles of $YbRh_2Si_2$ at 14 K sufficiently below the single-ion Kondo temperature T_K and at room temperature. As a reference for the *small* FS, we additionally measured the EOND of $YbCo_2Si_2$ and compared it to the one obtained by band-structure calculations. In comparison to the small FS reference $YbCo_2Si_2$, the electron density in $YbRh_2Si_2$ shows drastic signatures of reconstruction at low temperature upon cooling below T_K. These changes in the EOND may be attributed to the emergence of heavy $4f$-derived bands due to the formation of a coherent Kondo lattice. In stark contrast to the EOND of $YbCo_2Si_2$, which remains nearly unchanged between 14 and 300 K, the EOND of $YbRh_2Si_2$ shows strong modifications upon heating. At room temperature, the EOND of $YbRh_2Si_2$, and thus its FS, strongly resemble the reference of a *small* FS established from $YbCo_2Si_2$. Our results

show clear evidence of the long-sought Kondo crossover in $YbRh_2Si_2$ from the itinerant $4f$ moment at low temperatures due to the emergence of coherence in the Kondo lattice towards the localized $4f$ moment far above T_K. The temperature scale of this crossover can be narrowed down to about 100–300 K.

ACKNOWLEDGMENTS

The synchrotron radiation experiments were performed with the approval of the Japan Synchrotron Radiation Research Institute (JASRI) (Proposals No. 2015B1310, No. 2016A1371, No. 2016B1299, and No. 2017B1422). We gratefully acknowledge support from DFG Grants No. KR3831/5-1 and No. GE602/4-1 and the Research Training Group GRK 1621 and SFB 1143 (Project-id 247310070). D.V.V. acknowledges financial support from the Spanish Ministry of Economy (MAT-2017-88374-P).

D.V.V., K.Ku., and A.K. designed research; K.Kl., C.K., S.S., and C.G. grew and characterized the samples; A.K., M.G., K.Ku., and D.V.V. performed the Compton scattering experiments; theoretical studies were performed by M.G., Y.K., and K.Ku.; operation of the Compton scattering facility was carried out by A.K. and Y.S.; the obtained results were discussed together with C.L., Y.K., C.G., and Y.S.; and the manuscript was written by M.G. and K.Ku.

[1] G. R. Stewart, Heavy-fermion systems, Rev. Mod. Phys. **56**, 755 (1984).

[2] G. R. Stewart, Non-Fermi-liquid behavior in d- and f-electron metals, Rev. Mod. Phys. **73**, 797 (2001).

[3] F. Steglich, J. Aarts, C. D. Bredl, W. Lieke, D. Meschede, W. Franz, and H. Schäfer, Superconductivity in the Presence of Strong Pauli Paramagnetism: $CeCu_2Si_2$, Phys. Rev. Lett. **43**, 1892 (1979).

[4] P. F. S. Rosa, J. Kang, Y. Luo, N. Wakeham, E. D. Bauer, F. Ronning, Z. Fisk, R. M. Fernandes, and J. D. Thompson, Competing magnetic orders in the superconducting state of heavy-fermion $CeRhIn_5$, Proc. Natl. Acad. Sci. USA **114**, 5384 (2017).

[5] H. v. Löhneysen, A. Rosch, M. Vojta, and P. Wölfle, Fermi-liquid instabilities at magnetic quantum phase transitions, Rev. Mod. Phys. **79**, 1015 (2007).

[6] O. Trovarelli, C. Geibel, S. Mederle, C. Langhammer, F. M. Grosche, P. Gegenwart, M. Lang, G. Sparn, and F. Steglich, $YbRh_2Si_2$: Pronounced Non-Fermi-Liquid Effects above a Low-Lying Magnetic Phase Transition, Phys. Rev. Lett. **85**, 626 (2000).

[7] Q. Si, S. Rabello, K. Ingersent, and J. L. Smith, Locally critical quantum phase transitions in strongly correlated metals, Nature (London) **413**, 804 (2001).

[8] J. Custers, P. Gegenwart, H. Wilhelm, K. Neumaier, Y. Tokiwa, O. Trovarelli, C. Geibel, F. Steglich, C. Pépin, and P. Coleman, The break-up of heavy electrons at a quantum critical point, Nature (London) **424**, 524 (2003).

[9] R. M. Martin, The Fermi surface and Fermi liquid properties of periodic Kondo and mixed valence systems, J. Appl. Phys. **53**, 2134 (1982).

[10] J. M. Luttinger, Fermi surface and some simple equilibrium properties of a system of interacting fermions, Phys. Rev. **119**, 1153 (1960).

[11] Y. Ōnuki and R. Settai, De Haas–van Alphen effect and Fermi surface properties in rare earth and actinide compounds, Low Temp. Phys. **38**, 89 (2012).

[12] P. M. C. Rourke, A. McCollam, G. Lapertot, G. Knebel, J. Flouquet, and S. R. Julian, Magnetic-Field Dependence of the $YbRh_2Si_2$ Fermi Surface, Phys. Rev. Lett. **101**, 237205 (2008).

[13] H. Pfau, R. Daou, S. Lausberg, H. R. Naren, M. Brando, S. Friedemann, S. Wirth, T. Westerkamp, U. Stockert, P. Gegenwart, C. Krellner, C. Geibel, G. Zwicknagl, and F. Steglich, Interplay between Kondo Suppression and Lifshitz Transitions in $YbRh_2Si_2$ at High Magnetic Fields, Phys. Rev. Lett. **110**, 256403 (2013).

[14] R. Daou, C. Bergemann, and S. R. Julian, Continuous Evolution of the Fermi Surface of $CeRu_2Si_2$ across the Metamagnetic Transition, Phys. Rev. Lett. **96**, 026401 (2006).

[15] K. Miyake and H. Ikeda, True meaning of localized f-electrons measured by dHvA experiments in Ce-based heavy fermion metals, J. Phys. Soc. Jpn. **75**, 033704 (2006).

[16] S. Burdin, A. Georges, and D. R. Grempel, Coherence Scale of the Kondo Lattice, Phys. Rev. Lett. **85**, 1048 (2000).

[17] P. Coleman, Heavy fermions: Electrons at the edge of magnetism, in *Handbook of Magnetism and Advanced Magnetic Materials* (Wiley, New York, 2007).

[18] D. Vasumathi, B. Barbiellini, A. A. Manuel, L. Hoffmann, T. Jarlborg, R. Modler, C. Geibel, F. Steglich, and M. Peter, Fermi surface of $CeCu_2Si_2$ by 2D angular correlation of positron annihilation radiation, Phys. Rev. B **55**, 11714 (1997).

[19] J. D. Denlinger, G.-H. Gweon, J. W. Allen, C. G. Olson, M. B. Maple, J. L. Sarrao, P. E. Armstrong, Z. Fisk, and H. Yamagami, Comparative study of the electronic structure of XRu_2Si_2: Probing the Anderson lattice, J. Electron. Spectrosc. Relat. Phenom. **117-118**, 347 (2001).

[20] A. Koitzsch, S. V. Borisenko, D. Inosov, J. Geck, V. B. Zabolotnyy, H. Shiozawa, M. Knupfer, J. Fink, B. Büchner, E. D. Bauer, J. L. Sarrao, and R. Follath, Hybridization effects in $CeCoIn_5$ observed by angle-resolved photoemission, Phys. Rev. B **77**, 155128 (2008).

[21] S. Jang, J. D. Denlinger, J. W. Allen, V. S. Zapf, M. B. Maple, J. N. Kim, B. G. Jang, and J. H. Shim, Evolution of the Kondo lattice electronic structure above the transport coherence temperature, Proc. Natl. Acad. Sci. USA **117**, 23467 (2020).

[22] Q. Y. Chen, D. F. Xu, X. H. Niu, J. Jiang, R. Peng, H. C. Xu, C. H. P. Wen, Z. F. Ding, K. Huang, L. Shu *et al.*, Direct observation of how the heavy-fermion state develops in $CeCoIn_5$, Phys. Rev. B **96**, 045107 (2017).

[23] S. Danzenbächer, D. V. Vyalikh, K. Kummer, C. Krellner, M. Holder, M. Höppner, Y. Kucherenko, C. Geibel, M. Shi, L. Patthey, S. L. Molodtsov, and C. Laubschat, Insight into the f-Derived Fermi Surface of the Heavy-Fermion Compound $YbRh_2Si_2$, Phys. Rev. Lett. **107**, 267601 (2011).

[24] K. Kummer, S. Patil, A. Chikina, M. Güttler, M. Höppner, A. Generalov, S. Danzenbächer, S. Seiro, A. Hannaske, C. Krellner

et al., Temperature-Independent Fermi Surface in the Kondo Lattice $YbRh_2Si_2$, Phys. Rev. X **5**, 011028 (2015).

[25] A. Koizumi, G. Motoyama, Y. Kubo, T. Tanaka, M. Itou, and Y. Sakurai, f Electron Contribution to the Change of Electronic Structure in $CeRu_2Si_2$ with Temperature: A Compton Scattering Study, Phys. Rev. Lett. **106**, 136401 (2011).

[26] U. Köhler, N. Oeschler, F. Steglich, S. Maquilon, and Z. Fisk, Energy scales of $Lu_{1-x}Yb_xRh_2Si_2$ by means of thermopower investigations, Phys. Rev. B **77**, 104412 (2008).

[27] S. Ernst, S. Kirchner, C. Krellner, C. Geibel, G. Zwicknagl, F. Steglich, and S. Wirth, Emerging local Kondo screening and spatial coherence in the heavy-fermion metal $YbRh_2Si_2$, Nature (London) **474**, 362 (2011).

[28] D. Leuenberger, J. A. Sobota, S.-L. Yang, H. Pfau, D.-J. Kim, S.-K. Mo, Z. Fisk, P. S. Kirchmann, and Z.-X. Shen, Dehybridization of f and d states in the heavy-fermion system $YbRh_2Si_2$, Phys. Rev. B **97**, 165108 (2018).

[29] G. Dionicio, H. Wilhelm, G. Sparn, J. Ferstl, C. Geibel, and F. Steglich, Electrical resistivity of $YbRh_2Si_2$ at high pressure, Phys. B (Amsterdam, Neth.) **359-361**, 50 (2005).

[30] P. Gegenwart, J. Custers, C. Geibel, K. Neumaier, T. Tayama, K. Tenya, O. Trovarelli, and F. Steglich, Magnetic-Field Induced Quantum Critical Point in $YbRh_2Si_2$, Phys. Rev. Lett. **89**, 056402 (2002).

[31] A. Koizumi, Y. Kubo, G. Motoyama, T. Yamamura, M. Itou, and Y. Sakurai, Visual understanding of the hidden-order transition in URu_2Si_2 by high-resolution x-ray Compton scattering, Phys. Rev. B **92**, 125112 (2015).

[32] C. Krellner, S. Taube, T. Westerkamp, Z. Hossain, and C. Geibel, Single-crystal growth of $YbRh_2Si_2$ and $YbIr_2Si_2$, Philos. Mag. **92**, 2508 (2012).

[33] C. Klingner, C. Krellner, M. Brando, C. Geibel, F. Steglich, D. V. Vyalikh, K. Kummer, S. Danzenbächer, S. L. Molodtsov, C. Laubschat, T. Kinoshita, Y. Kato, and T. Muro, Evolution of magnetism in $Yb(Rh_{1-x}Co_x)_2Si_2$, Phys. Rev. B **83**, 144405 (2011).

[34] D. G. Lock, V. H. C. Crisp, and R. N. West, Positron annihilation and Fermi surface studies: A new approach, J. Phys. F: Met. Phys. **3**, 561 (1973).

[35] M. Cooper, P. Mijnarends, N. Shiotani, N. Sakai, and A. Bansil, *X-Ray Compton Scattering*, Oxford Series on Synchrotron Radiation (Oxford University Press, New York, 2004).

[36] Y. Tanaka, Y. Sakurai, A. T. Stewart, N. Shiotani, P. E. Mijnarends, S. Kaprzyk, and A. Bansil, Reconstructed three-dimensional electron momentum density in lithium: A Compton scattering study, Phys. Rev. B **63**, 045120 (2001).

[37] C. Klingner, C. Krellner, M. Brando, C. Geibel, and F. Steglich, Magnetic behavior of the intermetallic compound $YbCo_2Si_2$, New J. Phys. **13**, 083024 (2011).

[38] N. Mufti, K. Kaneko, A. Hoser, M. Gutmann, C. Geibel, C. Krellner, and O. Stockert, Unique magnetic structure of $YbCo_2Si_2$, Phys. Rev. B **94**, 045116 (2016).

[39] M. Güttler, K. Kummer, S. Patil, M. Höppner, A. Hannaske, S. Danzenbächer, M. Shi, M. Radovic, E. Rienks, C. Laubschat, C. Geibel, and D. V. Vyalikh, Tracing the localization of $4f$ electrons: Angle-resolved photoemission on $YbCo_2Si_2$, the stable trivalent counterpart of the heavy-fermion $YbRh_2Si_2$, Phys. Rev. B **90**, 195138 (2014).

[40] J. A. Hodges, Magnetic Ordering of Ytterbium in $YbCo_2Si_2$ and $YbFe_2Si_2$, Europhys. Lett. **4**, 749 (1987).

[41] K. Koepernik and H. Eschrig, Full-potential nonorthogonal local-orbital minimum-basis band-structure scheme, Phys. Rev. B **59**, 1743 (1999).

[42] P. Reiss, P. M. C. Rourke, G. Zwicknagl, F. M. Grosche, and S. Friedemann, $LuRh_2Si_2$: Sensitivity of the Fermi surface to the Si z-position, Phys. Status Solidi B **250**, 498 (2013).

[43] S. Friedemann, S. K. Goh, P. M. C. Rourke, P. Reiss, M. L. Sutherland, F. M. Grosche, G. Zwicknagl, and Z. Fisk, Electronic structure of $LuRh_2Si_2$: 'small' Fermi surface reference to $YbRh_2Si_2$, New J. Phys. **15**, 093014 (2013).

[44] A. Chikina, M. Höppner, S. Seiro, K. Kummer, S. Danzenbächer, S. Patil, A. Generalov, M. Güttler, Y. Kucherenko, E. V. Chulkov *et al.*, Strong ferromagnetism at the surface of an antiferromagnet caused by buried magnetic moments, Nat. Commun. **5**, 3171 (2014).

[45] M. Güttler, A. Generalov, M. M. Otrokov, K. Kummer, K. Kliemt, A. Fedorov, A. Chikina, S. Danzenbächer, S. Schulz, E. V. Chulkov *et al.*, Robust and tunable itinerant ferromagnetism at the silicon surface of the antiferromagnet $GdRh_2Si_2$, Sci. Rep. **6**, 24254 (2016).

[46] The deviation from exactly 1.0 hole is due to a rounding error made in the input of the band-structure code where we fixed the occupancy of the unpolarized $4f$ shell to 0.93×14 electrons. This results in 0.02 excess electrons in the $4f$ orbital, which are therefore missing in the valence band.

[47] S. Friedemann, S. Wirth, N. Oeschler, C. Krellner, C. Geibel, F. Steglich, S. MaQuilon, Z. Fisk, S. Paschen, and G. Zwicknagl, Hall effect measurements and electronic structure calculations on $YbRh_2Si_2$ and its reference compounds $LuRh_2Si_2$ and $YbIr_2Si_2$, Phys. Rev. B **82**, 035103 (2010).

[48] Y. Sakurai, M. Itou, B. Barbiellini, P. E. Mijnarends, R. S. Markiewicz, S. Kaprzyk, J.-M. Gillet, S. Wakimoto, M. Fujita, S. Basak *et al.*, Imaging doped holes in a cuprate superconductor with high-resolution Compton scattering, Science **332**, 698 (2011).

[49] K. Kummer, C. Geibel, C. Krellner, G. Zwicknagl, C. Laubschat, N. B. Brookes, and D. V. Vyalikh, Similar temperature scale for valence changes in Kondo lattices with different Kondo temperatures, Nat. Commun. **9**, 2011 (2018).

[50] See Figs. S1 and S2 and Note 1 in Supplemental Material at http://link.aps.org/supplemental/10.1103/PhysRevB.103.115126 for a discussion of the Fermi surface topology of $YbCo_2Si_2$ with varying distance between the Co and Si layers and a comparison to $LuRh_2Si_2$ [12,42,43].

[51] See Note 2 in Supplemental Material at http://link.aps.org/supplemental/10.1103/PhysRevB.103.115126 for a discussion of possible overshooting effects induced by the direct Fourier transform method and subsequent Lock-Crisp-West folding. Figure S3 in Supplemental Material shows the statistical error propagation through the reconstruction algorithm into the EONDs of $YbRh_2Si_2$, which was derived following the method described in Ref. [31].

[52] Figure S2 in Supplemental Material at http://link.aps.org/supplemental/10.1103/PhysRevB.103.115126 depicts the calculated partial contributions of the individual Fermi surface sheets to the total EOND in $YbCo_2Si_2$.

[53] See Fig. S4 in Supplemental Material at http://link.aps.org/supplemental/10.1103/PhysRevB.103.115126 comparing the Fermi surfaces of $YbCo_2Si_2$ and $YbRh_2Si_2$, both calculated for a fixed $4f^{13}$ configuration.

[54] See Note 3 in Supplemental Material at http://link.aps.org/supplemental/10.1103/PhysRevB.103.115126 for a discussion of the dips in the EOND in $YbRh_2Si_2$. As further discussed in the Supplemental Material Note, the minor differences between the high-temperature EONDs of both compounds might result from a residual f-d hybridization in $YbRh_2Si_2$ even at room temperature [28] in conjunction with a nontrivial energy- or possibly momentum-dependent crossover temperature of the lattice Kondo effect [61].

[55] See Fig. S5 in Supplemental Material at http://link.aps.org/supplemental/10.1103/PhysRevB.103.115126 for a comparison of EONDs resulting from a compensated or uncompensated Fermi surface in $YbRh_2Si_2$ at room temperature.

[56] A. B. Sutton, P. M. C. Rourke, V. Taufour, A. McCollam, G. Lapertot, G. Knebel, J. Flouquet, and S. R. Julian, Observation of the J-sheet of the Fermi surface of $YbRh_2Si_2$, Phys. Status Solidi B **247**, 549 (2010).

[57] Fig. S7 and Note 4 in Supplemental Material at http://link.aps.org/supplemental/10.1103/PhysRevB.103.115126 schematically illustrate the proposed renormalization of the doughnut $\mathcal{D}$ and jungle-gym $\mathcal{J}$ as derived from a simplified hybridization model based on the periodic Anderson model [62–64].

[58] M. Güttler, A. Generalov, S. I. Fujimori, K. Kummer, A. Chikina, S. Seiro, S. Danzenbächer, Y. M. Koroteev, E. V. Chulkov, M. Radovic *et al.*, Divalent $EuRh_2Si_2$ as a reference for the Luttinger theorem and antiferromagnetism in trivalent heavy-fermion $YbRh_2Si_2$, Nat. Commun. **10**, 796 (2019).

[59] H. C. Choi, B. I. Min, J. H. Shim, K. Haule, and G. Kotliar, Temperature-Dependent Fermi Surface Evolution in Heavy Fermion $CeIrIn_5$, Phys. Rev. Lett. **108**, 016402 (2012).

[60] See Note 5 in Supplemental Material at http://link.aps.org/supplemental/10.1103/PhysRevB.103.115126 for a more detailed discussion of characteristic temperature scales in $YbRh_2Si_2$ and, more generally, in Kondo lattices [6,21,24,27,28,59,61,65].

[61] A. Benlagra, T. Pruschke, and M. Vojta, Finite-temperature spectra and quasiparticle interference in Kondo lattices: From light electrons to coherent heavy quasiparticles, Phys. Rev. B **84**, 195141 (2011).

[62] A. C. Hewson, *The Kondo Problem to Heavy Fermions*, Cambridge Studies in Magnetism (Cambridge University Press, Cambridge, UK, 1993).

[63] H. J. Im, T. Ito, H.-D. Kim, S. Kimura, K. E. Lee, J. B. Hong, Y. S. Kwon, A. Yasui, and H. Yamagami, Direct Observation of Dispersive Kondo Resonance Peaks in a Heavy-Fermion System, Phys. Rev. Lett. **100**, 176402 (2008).

[64] D. V. Vyalikh, S. Danzenbächer, Y. Kucherenko, K. Kummer, C. Krellner, C. Geibel, M. G. Holder, T. K. Kim, C. Laubschat, M. Shi *et al.*, k Dependence of the Crystal-Field Splittings of $4f$ States in Rare-Earth Systems, Phys. Rev. Lett. **105**, 237601 (2010).

[65] S. Seiro, L. Jiao, S. Kirchner, S. Hartmann, S. Friedemann, C. Krellner, C. Geibel, Q. Si, F. Steglich, and S. Wirth, Evolution of the Kondo lattice and non-Fermi liquid excitations in a heavy-fermion metal, Nat. Commun. **9**, 3324 (2018).